

COMMUNICATIONS

Coherence in polyatomic photodissociation: Aligned O(³P) from photodissociation of NO₂ at 212.8 nmMusahid Ahmed, Darcy S. Peterka, and Allan S. Bracker^{a)}*Chemical Sciences Division, Ernest Orlando Lawrence Berkeley National Laboratory, Berkeley, California 94720*

Oleg S. Vasyutinskii

*Ioffe Physico-Technical Institute, Russian Academy of Sciences, 194021 St. Petersburg, Russia*Arthur G. Suits^{b)}*Chemical Sciences Division, Ernest Orlando Lawrence Berkeley National Laboratory, Berkeley, California 94720*

(Received 24 November 1998; accepted 23 December 1998)

Strong orbital alignment is observed in the ground-state oxygen atom following photodissociation of NO₂ at 212.8 nm using ion imaging. The imaging method allows for investigation of the angular distribution of this alignment, providing insight into the dynamics in the frame of the molecule. The results are analyzed using a rigorous quantum mechanical theory yielding alignment parameters having direct physical significance. This alignment is dominated by a strong incoherent parallel contribution. In addition, the results reveal direct evidence of coherence between parallel and perpendicular contributions to the excitation of a polyatomic molecule, showing that the electron cloud in the recoiling atom “remembers” the original molecular plane. © 1999 American Institute of Physics. [S0021-9606(99)02309-0]

In a classic 1968 paper,¹ Van Brunt and Zare predicted that photodissociation by polarized light could give rise to atoms having polarized orbitals, and the polarization of these orbitals could be analyzed to yield insight into the dynamics of the photochemical event. This prediction, realized in 1980,^{2,3} concerned the total alignment averaged over all recoil directions. The late 1980s saw a burst of interest in related phenomena when it was simultaneously realized in several laboratories that Doppler lineshapes obtained for molecular photofragments using polarized lasers contained additional information on the correlation between the recoil direction and the polarization of the rotational angular momentum ($\mathbf{v}-\mathbf{J}$ correlation), in effect, showing the *angular distribution* of this angular momentum polarization.^{4,5} Soon after, the ion imaging technique⁶ emerged as a powerful alternative to the Doppler approaches for obtaining detailed insight into photochemical problems.

With the development of the imaging method, observations of the angular distribution of atomic orbital polarization in photodissociation have begun to appear more frequently.⁷⁻⁹ However, the semiclassical approaches^{4,5} developed for treating the high- J cases relevant for product rotational angular momentum were not readily adapted to rigorous treatment of the low- J case of atomic orbital alignment. As a result, quantum mechanical effects have often been neglected in recent angle-resolved studies, although

these effects can be very important. Coherence effects in atomic alignment, for example, have been the subject of considerable work in angle-averaged studies in photodissociation¹⁰⁻¹⁵ as well as in collision studies¹⁶ in recent years, but in principle, the coherence contribution cannot be isolated from incoherent contributions in these studies. A full appreciation of the opportunities for exploiting atomic orbital polarization to probe coherence phenomena in angle-resolved photochemistry studies is only now beginning to emerge.^{17,18} Analogous effects for polarization of *rotational* angular momentum in molecular photofragments have been the subject of a great deal of study (see Ref. 19 and other references, for examples), but these phenomena generally reveal fundamentally different aspects of the photodissociation dynamics.

We have recently developed a rigorous quantum mechanical approach to treating angular momentum polarization in photodissociation as manifested in Doppler profiles²⁰ and in ion image data^{17,21,22} based on the work of Siebbeles *et al.*,²³ directly connecting the experimental results to alignment parameters having explicit physical significance. These parameters distinctly characterize both the coherent and incoherent contributions, as well as the symmetry of the transition involved, either parallel or perpendicular. The initial application of these methods^{17,21,22} was to the case of Cl₂ dissociation, in which direct evidence of a coherent perpendicular contribution to the photodissociation event was shown. In the report, we present measurements of the angular distribution of orbital alignment for the ground-state oxygen atom from photodissociation of NO₂ at 212.8 nm ob-

^{a)}Present address: Naval Research Laboratory, 4555 Overlook Ave. SW, Washington, DC 20375.

^{b)}Author to whom correspondence should be addressed.

TABLE I. Total alignment for the three spin-orbit states of $O(^3P_j)$.

State	$(I_{ }-I_{\perp})/(I_{ }+2I_{\perp})$
$O(^3P_2)$	0.010 ± 0.041
$O(^3P_1)$	0.088 ± 0.025
$O(^3P_0)$	0.016 ± 0.033

tained using the velocity map imaging technique.²⁴ These results represent the first observation of coherent features characteristic of photodissociation of nonlinear polyatomic molecules.

The molecular beam apparatus, described in detail in a recent publication,²⁵ consists of a skimmed molecular beam crossed by counterpropagating photolysis and probe lasers on the axis of an imaging time-of-flight mass spectrometer. The molecular beam was produced by expanding a 5% mixture of NO_2/O_2 seeded in helium from a piezoelectric pulsed valve. The photolysis laser was produced as the fifth harmonic of an Nd-yttrium-aluminum garnet (Nd-YAG) laser at 212.8 nm. The three fine-structure components of the ground-state oxygen atom product were probed near 226 nm. The probe transition²⁶ is a two-photon $2p \rightarrow 3p$ transition in which the three closely spaced upper-state fine-structure components are encompassed in the scan across the Doppler profile. Polarization of both the probe and photolysis lasers were independently rotated using waveplates. The resulting O^+ ions were accelerated toward an 80-mm diameter dual microchannel plate (MCP) coupled to a phosphor screen and imaged on a fast scan charge-coupled device camera with integrating video recorder (Data Design AC-101M). Four experimental configurations were employed to probe the atomic alignment: the photolysis laser polarization was parallel or perpendicular to the detector plane. The probe laser polarization was then fixed either parallel or perpendicular to the photolysis polarization.

Careful measurement of the total laboratory frame alignment is useful to scale the image data accurately. This data is shown in Table I for the three spin-orbit states of the product ground-state oxygen atom, along with the total relative value of the alignment implied by these values. Table I shows a negligible alignment for the $O(^3P_2)$ ground state, strong alignment of the $O(^3P_1)$, and the expected absence of alignment in the $O(^3P_0)$. Ion image data for the $O(^3P_1)$ product are shown in Fig. 1 for two different relative polarizations of the probe and photolysis lasers. The images contain both the angular and translational energy release distributions for the O atom product, the latter of which maps the internal energy distribution in the NO cofragment (by momentum and energy conservation). This kinetic energy distribution is shown in Fig. 2. The outer ring corresponds to production of NO peaking near $v=4$. The inner rings represent higher vibrational levels of NO, peaking near $v=10-11$ as shown. This bimodal translational energy distribution likely arises owing to dissociation via crossing to another potential surface. The spin-orbit distributions are quite distinct for the fast and slow contributions; this aspect of the problem will be the subject of a future study. The angular distributions are dominated by the population contribution, characterized by the familiar an-

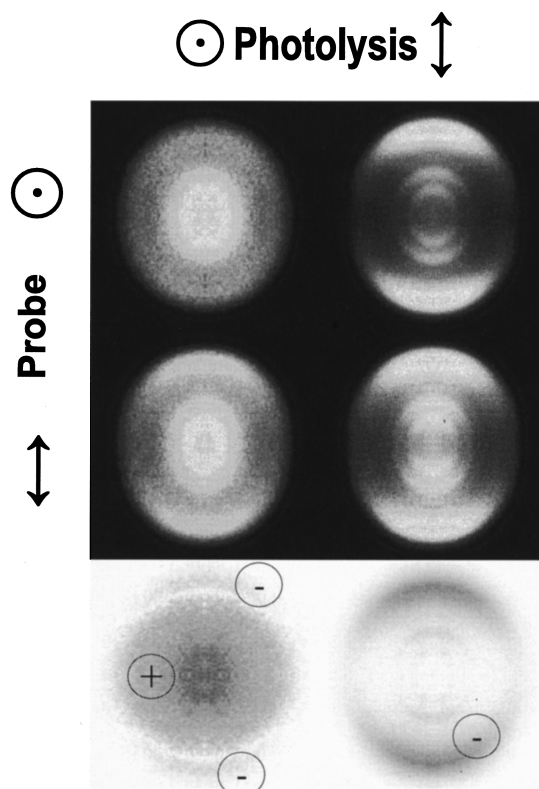


FIG. 1. Data images for $O(^3P_1)$ from photodissociation of NO_2 at 212.8 nm. Upper panel, experimental data for indicated combinations of photolysis and probe laser polarizations. Lower panel, difference images obtained from data representing alignment angular distributions. The background in the difference images is zero, difference signal is either positive or negative as indicated.

isotropy parameter β . Changes in the image with a change in probe laser polarization are a direct consequence of the orbital alignment, since the probe transition depends strongly on the relative orientation of the probe polarization and the atomic orbital in the recoiling atom. The angular distribution of the orbital alignment can be isolated from the larger total

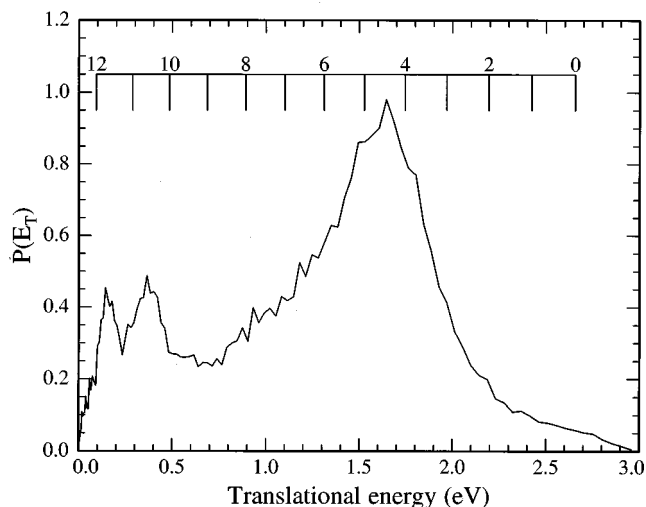


FIG. 2. Total translational energy distribution for $O(^3P_1)$ from images in Fig. 1. The comb shows the energy for the indicated vibrational level of a rotationless NO cofragment.

population signals by taking differences of the images for two different probe polarization directions.¹⁷ This is shown in the lower panel of Fig. 1. These images of the alignment angular distribution can be characterized by four alignment parameters, α_2 , s_2 , η_2 , and γ_2 , representing distinct physical mechanisms in the photodissociation process: α_2 and s_2 together are evidence of incoherent excitation mechanisms.²⁰ The limiting case of $\alpha_2 = 2s_2$ represents pure incoherent perpendicular excitation, while $s_2 = -\alpha_2$ represents pure incoherent parallel excitation. The remaining two parameters characterize the coherent contributions: η_2 for coherent perpendicular excitation, and γ_2 for coherent excitation of perpendicular and parallel transitions. Basis images corresponding to each of the distinct photolysis mechanisms have been developed, providing a means of fitting the results to extract the alignment parameters.^{17,21,22} A detailed quantitative analysis of this data in terms of these alignment parameters will require line-strength factors for the probe transition which are not yet available. However, qualitative insight may be obtained from the results directly, as we have shown in the Cl₂ case.²¹

In the present case, owing to the presence of the bimodal translational energy distributions, we have chosen to fit the image data by examining the angular behavior of the outer ring of the experimental distributions in the two geometries rather than attempting to fit the entire images. For simplicity, the inner rings are thus neglected in this analysis of the alignment and coherences. The angular dependence of the outer rings was fitted using basis curves developed from the simulated images shown in Ref. 17. These basis curves are generated on the same grid as the data images, resulting in some numerical “noise” in the basis curves. The basis curves and corresponding fits to the data are shown in Fig. 3. The fit shown in Fig. 3(B) was obtained setting the coherent contributions to zero. The result is a seriously inadequate simulation. It should be noted that both the shape and the magnitude of the difference curves constrain the fits, and both geometries I and II must be fitted simultaneously with the same parameters. When coherent contributions are included, as shown in Fig. 3(C), a satisfactory fit is readily obtained. The values of the parameters obtained from these fits are shown in Table II along with their limiting values and the range for each parameter. In the absence of further information on the probe line-strength factors, these are strictly relative values. However, estimates of the line-strength factors suggest that the absolute quantities are likely to be somewhat larger than the values indicated.

As is apparent from the results in Table I, the total alignment is significant only for the O(³P₁) state, and for this state it is substantial. The results of the analysis indicate that the dominant mechanism responsible for this alignment is an incoherent parallel excitation of the parent molecule. This is implied by values for α_2 and s_2 that are nearly equal and opposite in sign. Furthermore, this contribution reaches nearly half its limiting value. However, in addition to the incoherent contribution, we also find a significant nonzero value for the γ_2 parameter. For photolysis of NO₂ at 212.8 nm, the dominant excitation is to the 2 ²B₂ excited state, and the transition moment is in the plane of the molecule parallel

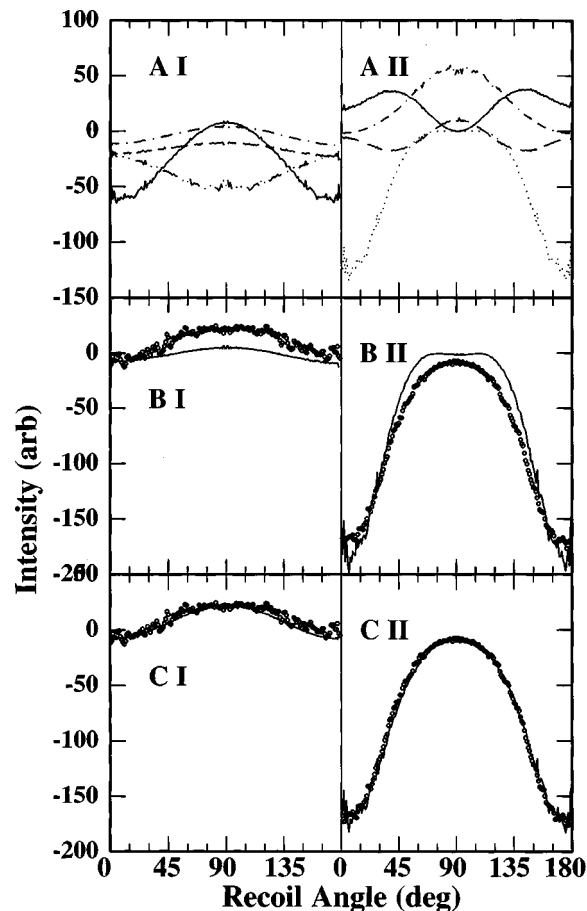


FIG. 3. (A) Basis curves showing contribution to angular distribution of alignment for each underlying mechanism. Incoherent parallel, —; Incoherent perpendicular, ---; Coherent perpendicular, -.-.; Coherent parallel/perpendicular, ...; (B) Data (circles) and best-fit simulation (solid line) obtained assuming no contribution from coherences; (C) Data (circles) and best-fit simulation (solid line) obtained including contribution from coherences. In all, “I” corresponds to photolysis laser perpendicular to detector plane, “II” corresponds to photolysis laser parallel to detector plane.

to the line joining the oxygen atoms.²⁷ The N–O bond in the ground-state equilibrium geometry makes an angle of 23° with this transition moment (see Fig. 4). In the frame of the recoiling oxygen atom (the “recoil frame”), the transition moment has both parallel and perpendicular components, i.e., projections both on Z_{rec} (the recoil direction) and the x -axis (defined to be perpendicular to Z_{rec} in the plane containing the transition moment μ). This is precisely the means by which coherences may be created in the angular momentum distribution in the oxygen atom. These coherences arise from the two contributions to the electronic transition in the recoil frame, resulting in a loss of cylindrical symmetry of

TABLE II. Alignment parameters obtained for O(³P₁) obtained from the fits shown in Fig. 3(C). Error values are 2 σ based on fits to three different data sets.

Parameter	Value	Range	Mechanism
s_2	0.044 ± 0.012	$-0.2, \dots, 0.1$	Incoherent and \perp
α_2	-0.036 ± 0.012	$-0.1, \dots, 0.2$	Incoherent and \perp
γ_2	-0.019 ± 0.008	$-0.21, \dots, 0.21$	Coherent and \perp
η_2	-0.0049 ± 0.008	$-0.3, \dots, 0.3$	Coherent \perp

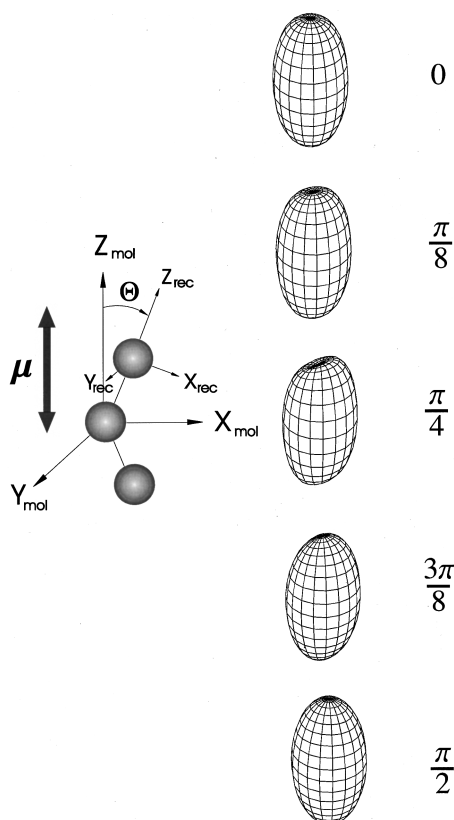


FIG. 4. On the left is a schematic view of NO_2 showing relative orientation of transition moment μ , molecular frame, and recoil frame. On the right are shown recoil-frame plots of the electron charge cloud for the product $\text{O}(^3P_1)$ atom based on the measured alignment parameters at indicated values of the angle Θ between the molecular Z axis and the recoil direction.

the electron cloud about the recoil direction. Figure 4 illustrates the shape of the electron cloud²⁸ implied by the measured alignment parameters for a range of recoil directions. The appearance of the electron cloud is dominated by the incoherent alignment contribution, giving the elongated shape to the charge distribution at all recoil angles. The coherent contribution shows up most clearly at $\Theta = \pi/4$, where the γ_2 contribution reaches a maximum. There, the azimuthal distortion of the electron cloud bears the imprint of the original molecular plane. The persistence of these coherences on the long (nanosecond) time scale of the experiment means that the oxygen atom “remembers” the original plane of the molecule even in the asymptotic region. We note that this is likely to be a common feature of polyatomic photodissociation, and is not specific to NO_2 . It is interesting to contrast this observation with coherence effects observed in photodissociation of diatomic molecules.^{18,21,22,29} In the diatomic case, coherent excitation of two dissociative states of different symmetry leads to quantum mechanical interference, yielding an electron cloud in the recoiling atom possessing azimuthal asymmetry, and observed as oscillations in

the angular distributions when probed by polarized lasers. In the polyatomic case, formally speaking the mechanism is the same: coherent excitation of states of different symmetry (in the recoil frame) leads to quantum mechanical interference. However, in the polyatomic case, the presence of these states of distinct symmetry arises directly from the nuclear symmetry in the molecule. This work represents the first observation of this phenomenon.

These alignment parameters can provide further detailed insight into the dissociation dynamics, including nonadiabatic interactions and contributions from long-range forces.^{17,20,21,22} However, these detailed investigations will require the line-strength factors mentioned above; these efforts are underway.

This work was supported by the Director, Office of Energy Research, Office of Basic Energy Sciences, Chemical Sciences Division of the U.S. Department of Energy under contract No. DE-ACO-3-76SF00098, and by a Cooperative Grant from the Civilian Research and Development Fund, CRDF Award RP1-223. We wish to acknowledge Dr. E. Wouters for helpful discussions. O.S.V. thanks the Advanced Light Source at LBNL for additional support during a recent visit to Berkeley.

- ¹R. J. Van Brunt and R. N. Zare, *J. Chem. Phys.* **48**, 4304 (1968).
- ²O. S. Vasyutinskii, *Sov. Phys. JETP* **31**, 428 (1980).
- ³E. W. Rothe, U. Krause, and R. Duren, *Chem. Phys. Lett.* **72**, 100 (1980).
- ⁴G. E. Hall *et al.*, *Phys. Rev. Lett.* **56**, 1671 (1986).
- ⁵R. N. Dixon, *J. Chem. Phys.* **85**, 1866 (1986).
- ⁶D. W. Chandler and P. L. Houston, *J. Chem. Phys.* **87**, 1445 (1987).
- ⁷Y. Mo *et al.*, *Phys. Rev. Lett.* **77**, 830 (1996).
- ⁸T. Suzuki *et al.*, *Chem. Phys. Lett.* **256**, 90 (1996).
- ⁹A. T. J. B. Eppink *et al.*, *J. Chem. Phys.* **108**, 1305 (1998).
- ¹⁰J. Vigué, J. A. Beswick, and M. Broyer, *J. Phys. (Paris)* **44**, 1225 (1983).
- ¹¹J. Vigué *et al.*, *J. Phys. Lett. (France)* **42**, (1981).
- ¹²M. Glass-Maujean and J. A. Beswick, *Phys. Rev. A* **36**, 1170 (1987).
- ¹³M. Glass-Maujean and J. A. Beswick, *J. Fac. Sci., Univ. Tokyo, Sect. 1* **85**, 983 (1989).
- ¹⁴M. Glass-Maujean and J. A. Beswick, *Phys. Rev. A* **38**, 5660 (1988).
- ¹⁵E. Flemming *et al.*, *J. Chem. Phys.* **103**, 4090 (1995).
- ¹⁶J. P. J. Dreissen and S. R. Leone, *J. Phys. Chem.* **96**, 6136 (1992).
- ¹⁷A. S. Bracker *et al.*, *Phys. Rev. Lett.* **80**, 1626 (1998).
- ¹⁸T. P. Rakitzis, S. A. Kandel, and R. N. Zare, *J. Chem. Phys.* **108**, 8291 (1998).
- ¹⁹J. R. Waldeck, J. F. Black, and R. N. Zare, *J. Chem. Phys.* **92**, 3519 (1990).
- ²⁰B. V. Picheyev, A. G. Smolin, and O. S. Vasyutinskii, *J. Phys. Chem.* **101**, 7614 (1997).
- ²¹A. S. Bracker, Ph.D. thesis, University of California, Berkeley, 1997.
- ²²A. S. Bracker *et al.*, *J. Chem. Phys.* (in press).
- ²³L. D. A. Siebbeles *et al.*, *J. Chem. Phys.* **100**, 3610 (1994).
- ²⁴A. T. J. B. Eppink and D. H. Parker, *Rev. Sci. Instrum.* **68**, 3477 (1997).
- ²⁵M. Ahmed *et al.*, *J. Chem. Phys.* **106**, 7617 (1997).
- ²⁶D. J. Bamford, M. J. Dyke, and W. K. Bishel, *Phys. Rev. A* **26**, 3497 (1987).
- ²⁷W. M. Uselman and E. K. C. Lee, *J. Chem. Phys.* **65**, 1948 (1975).
- ²⁸K. Blum, *Density Matrix Theory and Applications, Second Edition* (Plenum, New York, 1996).
- ²⁹T. P. Rakitzis *et al.*, *Science* **281**, 1346 (1998).